Earth Syst. Dynam. Discuss., https://doi.org/10.5194/esd-2018-87
Manuscript under review for journal Earth Syst. Dynam.
Discussion started: 1 March 2019

Earth System Dynamics Discussions
Open Access
EGU

Meeting climate targets by direct CO_2 injections: What price would the ocean have to pay?

Fabian Reith[1], Wolfgang Koeve[1], David P. Keller[1], Julia Getzlaff[1], and Andreas Oschlies[1]

[1]GEOMAR Helmholtz-Centre for Ocean Research Kiel, Düsternbrooker Weg 20, 24105 Kiel, Germany

Correspondence to: Fabian Reith (FReith@geomar.de)

Abstract. We investigate the climate mitigation potential and collateral effects of direct injections of captured CO_2 into the deep ocean as a possible means to close the gap between an intermediate CO_2 emissions scenario and a specific temperature target, such as the 1.5°C target aimed for by the Paris Agreement. For that purpose, a suite of approaches for controlling the amount of direct CO_2 injections at 3000m water depth are implemented in an Earth System Model of intermediate complexity.

Following the representative concentration pathway RCP4.5, which is a medium mitigation CO_2 emissions scenario, cumulative CO_2 injections required to meet the 1.5°C climate goal are found to be 390 Gt C by the year 2100 and 1562 Gt C at the end of simulations, by the year 3020. The latter includes a cumulative leakage of 602 Gt C that needs to be re-injected in order to sustain the targeted global mean temperature.

$CaCO_3$ sediment and weathering feedbacks reduce the required CO_2 injections that comply with the 1.5°C target by about 13 % in 2100 and by about 11 % at the end of the simulation.

With respect to the injection-related impacts we find that average pH values in the surface ocean are increased by about 0.13 to 0.18 units, when compared to the control run. In the model, this results in significant increases in potential coral reef habitats, i.e., the volume of the global upper ocean (0 to 130m depth) with omega aragonite > 3.4 and ocean temperatures between 21°C and 28°C, compared to the control run. The potential benefits in the upper ocean come at the expense of strongly acidified water masses at depth, with maximum pH reductions of about -2.37 units, relative to preindustrial, in the vicinity of the injection sites. Overall, this study demonstrates that massive amounts of CO_2 would need to be injected into the deep ocean in order to reach and maintain the 1.5°C climate target in a medium mitigation scenario on a millennium timescale, and that there is a trade-off between injection-related reductions in atmospheric CO_2 levels accompanied by reduced upper-ocean acidification and adverse effects on deep ocean chemistry, particularly near the injection sites.

1. Introduction

The Paris Agreement of December 2015 has set the political target of limiting global warming to well below 2°C, if not 1.5°C, above preindustrial levels (UNFCCC, 2015). Staying within the Paris target range is perceived as a safe limit that avoids dangerous anthropogenic climate change and ensures sustainable food production and economic development (Rock-

ström et al., 2009; Knutti et al., 2015; Rogelj et al., 2016). As a first step towards meeting the Paris climate goals, countries have outlined national post-2020 climate action plans by submitting their Nationally Determined Contributions (NDCs) to climate mitigation in order to meet the <2°C climate target (e.g., Clémençon, 2016). However, even if these NDCs are fully realized, it is estimated that a median warming of 2.6 to 3.1°C will occur by the year 2100 (Rogelj et al., 2016). Consequently, it is questionable whether conventional measures currently considered by individual states will be sufficient to reach and maintain the <2°C climate target (e.g., Horton et al., 2016).

The scientific rationale of such claims is based on observational records and results of climate models of varying complexity that have found a tight correlation between cumulative CO_2 emissions and global mean temperature (Allen et al., 2009; Matthews et al., 2009; MacDougall, 2016). From this transient climate response to cumulative carbon emissions (TCRE) it can be estimated that the total quota of CO_2 emissions from all sources (fossil fuel combustion, industrial processes and land-use change) that is compatible with a 1.5°C target will be used up in a few years at current emission rates (Knopf et al., 2017; Mengis et al., 2018), and for a 2°C target it is likely to be reached in the next 2 to 3 decades (Friedlingstein et al., 2014). Thus, the window of opportunity for deep and rapid decarbonization that would allow for such a climate target through emissions reduction alone is closing soon (Sanderson et al., 2016).

Given the very challenging and urgent nature of the task of reaching the agreed-upon Paris climate goals, unconventional methods are being discussed. Under specific consideration are negative emission technologies, i.e., measures that deliberately remove CO_2 from the atmosphere (e.g., Gasser et al., 2015) and store it somewhere else, e.g., in geological reservoirs or the deep ocean (e.g., IPCC, 2005). Negative emissions are already included in all realistic scenarios from integrated assessment models (IAMs) that limit global warming to <2°C or less above preindustrial levels (Collins et al., 2013; Rockström et al., 2016; Rogelj et al., 2016). However, none of the currently debated negative emissions technologies, such as bioenergy with carbon capture and storage (BECCS), direct air capture with carbon storage (DACCS) and enhanced weathering (EW), appears to have, regardless of the scenario, the potential to meet the <2°C target without significant impacts on land, energy, water or nutrient resources (Fuss et al., 2014; Smith et al., 2016; Williamson, 2016; Boysen et al., 2017).

One other option that has been considered is ocean carbon sequestration by direct injection of CO_2 into the deep ocean (e.g., Marchetti, 1977; Hoffert et al., 1979; Orr et al, 2001; Orr, 2004; IPCC, 2005; Reith et al., 2016). The CO_2 could be derived from point sources such as power plants or direct air capture facilities, and thereby contribute to the carbon sequestration part of CCS, DACCS or BECCS. Direct injection of CO_2 into the deep ocean can also be thought of as the deliberate acceleration of the oceanic uptake of atmospheric CO_2, which happens naturally via invasion and dissolution of CO_2 into the surface waters, albeit at a relatively slow rate limited by the sluggish ocean overturning circulation. On millennial timescales, about 65-80% of anthropogenic CO_2 is thought to be taken up by the ocean via gas exchange at the ocean surface and by entrainment of surface waters into the deep ocean. This portion rises to 73-93% on timescales of tens to hundreds of

millennia via neutralization of carbonic acid with sedimentary calcium carbonate ($CaCO_3$) (e.g., Archer et al., 2005; Zeebe, 2012). Directly injecting CO_2 into the deep ocean could speed up this natural process by directly accessing deep waters, some of which remain isolated from the atmosphere for hundreds or thousands of years (DeVries and Primeau, 2011; their Figure 12), and by bringing the anthropogenic CO_2 in closer contact with the sediment where carbonate compensation reactions occur. This would prevent anthropogenic CO_2 from having an effect on the climate in the near future, and accelerate eventual and nearly permanent removal via reaction with $CaCO_3$ sediments.

Despite the well-known potential of the ocean to take up and store carbon (e.g., Sarmiento and Toggweiler, 1984; Volk and Hoffert, 1985; Sabine et al., 2004;), direct CO_2 injection into the deep ocean is currently not allowed by the London Protocol and the Convention for the Protection of the Marine Environment of the North East Atlantic (OSPAR Convention) (Leung et al., 2014). A main concern that led to the current ban is that direct CO_2 injection will harm marine ecosystems in the deep sea, e.g., cold-water corals and sponge communities, at least close to the injection site (e.g., IPCC, 2005; Schubert et al., 2006; Gehlen et al., 2014). As emphasized by Keeling (2009) and Ridgwell et al. (2011) there are, however, trade-offs between injection-related damages in the deep ocean and benefits at the ocean surface via a reduction in atmospheric pCO_2 and a decrease in upper ocean acidification. These should be discussed in relation to other mitigation options, that probably all imply offsetting some local harm against global benefits. Our current study aims to inform such a debate by providing quantitative information about impacts on ocean carbonate chemistry caused by direct injection of CO_2 into the deep ocean as a potential measure to reach and maintain a specific temperature target as given by the Paris climate targets.

For this purpose, we consider direct injection of CO_2 into the deep ocean as 'oceanic CCS', deposing CO_2 from point sources such as fossil fuel or biomass-based power plants or direct air capture plants. We assume that aggressive emissions reduction has led from a business-as-usual CO_2 emission scenario to a world with intermediate CO_2 emissions such as the one represented by the Representative Concentration Pathway (RCP) 4.5. Model-predicted global mean surface air temperatures for the RCP 4.5 CO_2 emission scenario range between 1.7°C and 3.2°C in the year 2100 (Clarke et al., 2014), which is approximately in agreement with the warming after full achievement of current NDCs. Consequently, the 1.5°C climate target would not be reached under the RCP 4.5 scenario and is likely to be exceeded after the year 2050 (IPCC, 2014). We here explore the potential as well as collateral oceanic effects of 'oceanic CCS' as a means to fill the gap between emissions and climate impacts of the RCP 4.5 and the 1.5°C target of the Paris agreement. Due to the fact that we neglect the effects of non-CO_2 forcing agents in our injection experiments, our results provide a lower limit estimate, i.e. the cumulative CO_2 amount that would need to be at least injected into the deep ocean in order to comply with the desired target.

The paper is organized as follows: In section 2 we address the methodological framework by describing the UVic model and the experimental setup of our experiments. In section 3 the results and the discussion of our model simulations are presented. Section 4 outlines the conclusions.

Earth Syst. Dynam. Discuss., https://doi.org/10.5194/esd-2018-87
Manuscript under review for journal Earth Syst. Dynam.
Discussion started: 1 March 2019

2. Methods

2.1 Model description

The model used is version 2.9 of the University of Victoria Earth System Climate Model (UVic ESCM). It consists of three dynamically coupled main components: a three-dimensional general circulation ocean model based on the Modular Ocean Model MOM2 (Pacanowski, 1996) including a marine biogeochemical model (Keller et al., 2012), a dynamic-thermodynamic sea-ice model (Bitz and Lipscomb, 1999) and a $CaCO_3$-sediment model (Archer, 1996). The UVic ESCM further includes a terrestrial vegetation and carbon-cycle model (Meissner et al., 2003) based on the Hadley Center model TRIFFID (Top-down Representation of Interactive Foliage and Flora Including Dynamics) and the hydrological land component MOSES (Met Office Surface Exchange Scheme), and a one-layer atmospheric energy-moisture balance model (based on Fanning and Weaver, 1996). All components have a common horizontal resolution of 3.6° longitude x 1.8° latitude. The oceanic component has 19 vertical levels with thicknesses ranging from 50 m near the surface to 500 m in the deep ocean. Formulations of the air-sea gas exchange and seawater carbonate chemistry are based on the OCMIP abiotic protocol (Orr et al., 1999). Marine sediment processes of $CaCO_3$ burial and dissolution are simulated using a model of deep ocean sediment respiration (Archer, 1996).

2.2 Experimental design

For our default control run and injection experiments, the model has been spun up for 10,000 years under preindustrial atmospheric and astronomic boundary conditions and run from 1765 to 2005 using historical fossil-fuel and land-use carbon emissions (Keller et al., 2014). From the year 2006 onwards simulations are forced with CO_2 emissions according to the RCP 4.5 and the Extended Concentration Pathway (ECP) 4.5, which runs until the year 2500 (Meinshausen et al., 2011). This forcing includes CO_2-emissions from fossil fuel burning as well as land-use carbon emissions, e.g. from deforestation. After the year 2500, CO_2 emissions are assumed to decrease linearly until they cease at the end of the simulations in year 3020. In the default control run and injection experiments we do not apply greenhouse gas emissions other than CO_2, nor do we simulate the effect of sulfate aerosols or non-CO_2 effects of land use change. Further, prescribed monthly varying winds from the National Center for Environmental Prediction (NCEP) reanalysis are used together with a dynamical feedback from a first-order approximation of geostrophic wind anomalies associated with changing winds in a changing climate (Weaver et al., 2001).

Simulated CO_2 injections are based on the OCMIP carbon sequestration protocols (see Orr et al., 2001; Orr, 2004) and carried out in an idealized manner by adding CO_2 directly to the dissolved inorganic carbon (DIC) pool, thus neglecting any gravitational effects and assuming that the injected CO_2 instantaneously dissolves into seawater and is transported quickly away from the injection point and distributed homogenously over the entire model grid box with lateral dimensions of a

few hundred kilometers and many tens of meters in the vertical direction (Reith et al., 2016). Consequently, the formation of CO_2 plumes or lakes as well as the potential risk of fast rising CO_2 bubbles are neglected (IPCC, 2005; Bigalke et al., 2008).

The physical transport of the injected CO_2 and its transport pathways from the individual injection sites towards the surface of the ocean are tracked by means of inert 'dye' tracers (one per injection site). At the injections sites, these tracers are loaded at rates proportional to the amount of CO_2 injected. At the sea surface the tracers are subject to a loss to the atmosphere, which is computed in proportionality to the total CO_2 gas exchange and fractional contribution to total DIC of the respective tracer at the ocean surface. The sum of tracer loss to the atmosphere from the individual 'dye' tracers provides an estimate of the loss of injected carbon to the atmosphere.

Following Orr et al. (2001), Orr (2004) and Reith et al. (2016) CO_2 is injected at seven separate injection sites, which are defined as individual grid boxes near the Bay of Biscay (42.3°N, 16.2°W), New York (36.9°N, 66.6°W), Rio de Janeiro (27.9°S, 37.8°W), San Francisco (31.5°N, 131.4°W), Tokyo (33.3°N, 142.2°E), Jakarta (11.7°S, 102.6°E) and Mumbai (13.5°N, 63°E) (Reith et al., 2016; their Figure 1). Injected CO_2 is distributed equally among the seven injection sites. Direct CO_2 injections are carried out in the vertical grid box ranging from 2580 to 2990 m water depth (hereafter referred to as injection at 3000 m). Compared to shallower injection, this reduces leakage and increases retention time (e.g., Orr et al., 2001; Orr, 2004; Jain and Cao, 2005; Ridgwell et al., 2011; Reith et al., 2016). At this depth, liquid CO_2 is denser than seawater, which has the additional advantage that any undissolved droplets would sink to the bottom rather than rise to the surface.

2.3 Model experiments

Three conceptually different approaches for applying oceanic CCS are simulated using the UVic model: The first approach (*A1*) assumes that all anthropogenic CO_2 emissions are injected after a warming of 1.5°C is realized for the first time, the second approach (*A2*) injects, in every year, an amount of CO_2 that ensures that temperatures do not rise beyond the 1.5°C target, and the third approach (*A3*) injects an amount of CO_2 to ensure that atmospheric CO_2 concentrations follow the RCP/ECP 2.6 scenario as closely as possible. All idealized approaches are designed to counter the excessive emissions of the RCP 4.5 scenario by direct CO_2 injections into the deep ocean to reach and maintain a specific temperature target as given by the 1.5°C target until the end of this century and for another millennium. Injections in A2 (A3) are interrupted when the simulated annual mean surface air temperature (atmospheric pCO_2) falls below the respective climate target. We further study how the simulation of $CaCO_3$ sediment feedbacks and associated continental weathering modifies required CO_2-injections and its impacts on ocean biogeochemistry. Table 1 provides an overview of all conducted simulations and their set-up from the year 2006 onwards.

In the first approach (*A1*), all further CO_2 emissions of the RCP 4.5 scenario are completely re-directed to the injection sites after the global-mean surface air temperature has for the first time exceeded the 1.5°C target. Some committed warming

(e.g., Matthews and Caldeira, 2008; Gillet et al., 2011) occurs in these simulations due to past emissions and climate cycle feedbacks. This committed warming is at some point overlaid by leakage of injected CO_2 out of the ocean (e.g., Orr, 2004; Reith et al., 2016), as well as by oceanic and terrestrial carbon cycle feedbacks that lead to a CO_2 increase in the atmosphere and respective additional warming (see section 3.1). To diagnose the contribution from leakage, we design a leakage-free sensitivity simulation (*A1_ Comitw)*, in which CO_2 emissions are set to zero once the 1.5°C target is reached, and no CO_2 is injected into the deep ocean.

In contrast to the first approach, the second one (*A2)* keeps the global mean temperature at the defined threshold of 1.5°C, relative to preindustrial, by injecting as much CO_2 into the deep ocean as is necessary to maintain an annual mean temperature that is only 1.5°C above preindustrial levels. We diagnose this amount of CO_2 using the transient response to emissions (TCRE, Allen et al., 2009; Matthews et al., 2009; MacDougall, 2016) of our model and the difference of the modeled annual mean atmospheric temperature and the target temperature. CO_2 is only injected if the modeled temperature is above the target temperature. In order to avoid interference with seasonal and longer periodic fluctuations of atmospheric temperature (sensitivity experiments, not shown) we apply a running-mean averaging time scale of 1000 days. CO_2 injection rates required to reach the respective target are updated every 5 days, which is when the atmospheric and oceanic model components are coupled. The rate of CO_2 injection taken out of the atmosphere can be larger than the actual CO_2-emissions (RCP/ECP 4.5), i.e. constitute net negative CO_2 emissions.

In the third approach (*A3*), we inject the amount of CO_2 that is needed to follow the atmospheric CO_2 concentrations of the extended Representative Concentration Pathway RCP 2.6 and Extended Concentration Pathway ECP 2.6, which is a reference scenario that has been suggested to reach the <2°C climate target with a ≥66% probability (IPCC, 2014). From year 2500 onwards, the targeted atmospheric CO_2 concentration is held constant until the end of the simulations. Therefore, the model computes at every atmospheric time step the difference between its current simulated atmospheric CO_2 concentration, given the RCP 4.5 CO_2-emissions, and the targeted atmospheric CO_2 concentration from the RCP 2.6 pathway. This difference is used to diagnose the CO_2-injection needed to keep the model's atmospheric CO_2 concentrations as close as possible to the RCP 2.6 concentration pathway. A respective amount of CO_2 is injected and subtracted from the prescribed CO_2 emissions to the atmosphere, which eventually results in net negative emissions. We apply temporal averaging and update the required CO_2-injection every 5 days.

In sensitivity experiments (Table 1) we further investigate the effect of $CaCO_3$ sediment feedbacks and continental weathering on the cumulative CO_2 injections and on seawater carbonate chemistry for the different approaches. The effect of $CaCO_3$ sediment dissolution is thought to be relevant as CO_2 injected at depth may react relatively directly with sedimentary $CaCO_3$ and increase $CaCO_3$ dissolution near or downstream of the injection sites, resulting in an accelerated neutralization of this anthropogenic CO_2 compared to a situation where CO_2 slowly invades the ocean via air-sea gas exchange (Archer et al., 1998; IPCC, 2005). Therefore, we investigate the effect of $CaCO_3$ sediment feedbacks in our simulations by running the

model with and without a sediment sub-model. The global average percent of $CaCO_3$ in sediments in our "*sed*" simulations (section 3.2) is about 31 % in the year 2020 and compares well to about 34.5 % derived from observations as reported in Eby et al. (2009). To ensure that, in steady state (i.e., during the model spin-up), DIC and alkalinity are conserved, the UVic model with sediment module also has a simple representation of continental weathering to compensate the burial-related loss of DIC and alkalinity. From the model spin-up we diagnose the global terrestrial weathering flux of DIC as 0.12 Gt C yr^{-1}, and an alkalinity flux of 0.02 Pmol yr^{-1}. During the transient runs with sediment module, this weathering flux is held constant, whereas sedimentary $CaCO_3$ accumulation or dissolution is allowed to evolve freely. Consequently, ocean alkalinity and DIC adjust in response to interactions between seawater, injected CO_2, and sediments. Simulations with the sediment/weathering sub-model are based on a separate set of spin-up experiments (50 000 years), drift runs and historical simulation that all employ the sediment/weathering sub-model. Hereafter, simulations performed with the sediment/weathering model are referred to by the subscript "*sed*" (Table 1).

Relevant carbonate system parameters that are not computed at model run-time are derived offline for all simulations by means of the Matlab-version of *CO2SYS* (Lewis and Wallace, 1998; van Heuven et al., 2009; Koeve and Oschlies, 2012; currently available from http://cdiac.ess-dive.lbl.gov/ftp/co2sys), using carbonic acid dissociation constants of Mehrbach et al. (1973), as refitted by Dickson and Millero (1987), and other related thermodynamic constants (Millero, 1995).

3. Results and Discussion

3.1 Oceanic CCS and the 1.5°C climate target

Here, we present the cumulative mass of CO_2 injected in the default runs (without $CaCO_3$ sediments) of the different approaches and show how effective these are in reaching and maintaining the 1.5°C climate target.

In the default simulation of the first approach (*A1*) oceanic CCS starts in the year 2045 after the 1.5°C climate target has been exceeded for the first time at a corresponding atmospheric CO_2 concentration of about 466 ppmv (Figs. 1 a, b, c). Between years 2020 and 2045, about 278 Gt C have been emitted in form of CO_2 to the atmosphere, i.e. a small fraction of the 1242 Gt C of total emissions corresponding the extended RCP 4.5 scenario between years 2020 and 3020. From 2045 until year 3020, all CO_2 emissions (964 Gt C in total) are directly injected into the deep ocean (Fig. 1 a), resulting in zero anthropogenic CO_2 emissions into the atmosphere for the remaining simulation. After injection starts in year 2045, the atmospheric CO_2 concentration decreases, but only until the year 2341, when a minimum of about 409 ppmv is reached (Fig. 1 c). The increase of atmospheric CO_2 from year 2342 onwards is a result of leakage of CO_2 injected into the deep ocean earlier. By the end of the simulation, a total amount of 437 Gt C has leaked back into the atmosphere (Fig. 1 d). Thus, only about 55 % of the total mass injected (964 Gt C) remains in the ocean until year 3020. From 2078 onwards, the land perennially turns into a carbon source with a total carbon loss of about 21 Gt C to the atmosphere.

Earth Syst. Dynam. Discuss., https://doi.org/10.5194/esd-2018-87
Manuscript under review for journal Earth Syst. Dynam.
Discussion started: 1 March 2019

Global mean temperature, relative to preindustrial, oscillates around the 1.5°C climate target within ± 0.02°C after injections started until the year 2200. Until then, this approach (*A1*) is thus nearly successful in reaching and maintaining the 1.5°C climate target. Subsequently, however, global mean surface air temperature shows a slow increase of up to 0.02°C until 2341 although atmospheric CO_2 still decreases. This warming signal is owed to the lagged response of the deep ocean to previously increasing atmospheric CO_2, i.e. committed warming, resulting in a decline of the ocean heat uptake from the atmosphere and thus in an increase in the global mean temperature (Zickfeldt and Herrington, 2015; Zickfeldt et al., 2016). In this simulation (*A1*), this feedback mechanism (see also Fig. S1) is overlaid by increasing leakage of injected CO_2 back into the atmosphere, which becomes the dominating process for atmospheric warming as obvious from the atmospheric CO_2 increase after year 2342 (Figs. 1 c, d). Hence, the global mean air temperature shows a steeper increase until it reaches a maximum of about +2.2°C above preindustrial level at the end of the simulation (Fig. 1 b). Thus, on a millennial time scale, the *A1* simulation overshoots the 1.5°C climate target by about 0.7°C. By subtracting this diagnosed leakage of 437 Gt C from the cumulative CO_2 injections (964 Gt C), we determine the required CO_2 emission reduction (527 Gt C) (Fig. 1 e) relative to the RCP/ECP 4.5 scenario to comply with a global mean temperature of about +2.2°C, relative to preindustrial, on a thousand-year timescale.

Oceanic CCS in the second approach (*A2*) starts as well in 2045 (Figs. 1 a, c). Global mean temperature oscillates around the 1.5°C climate target until year 2300 (Fig. 1 b). These oscillations get smaller over time until global mean temperature essentially stays at 1.5°C until the end of the simulation. We find that the oscillations arise in the applied model from climate-sea-ice feedbacks under the near-term 1.5°C conditions (see Fig. S2). The terrestrial biosphere turns into a carbon source in 2061 and land-atmosphere carbon fluxes oscillate around zero until the end of the simulation. The total carbon loss from land to the atmosphere is about 75 Gt C. Atmospheric CO_2 concentrations show a continuous decline when global mean temperature is held at the aspired climate target (Figs. 1 b, c). This is caused by a decline in ocean heat uptake as mentioned above and consistent to an additional accumulation of heat in the atmosphere at constant atmospheric CO_2 concentrations (e.g., Zickfeldt and Herrington, 2015; Zickfeldt et al., 2016), and which, in our second approach, needs to be counteracted by further CO_2 injections into the deep ocean.

By the end of the *A2* run, cumulative CO_2 injections amount to about 1562 Gt C, which is about 600 Gt C (62 %) higher than in the *A1* simulation. This amount of additional CO_2-injections is needed in order to reduce global mean warming at the end of the thousand-year simulation from 2.2°C in run *A1* to 1.5°C in run *A2*. In the *A2* run, the diagnosed mass of injected CO_2 that has leaked into the atmosphere and has been reinjected into the deep ocean during the entire simulation adds up to about 607 Gt C until year 3020 (Fig. 1 d). Hence, about 61 % of the total mass injected (1562 Gt C) stays in the ocean. This results in a required CO_2 emission reduction of about 955 Gt C (Fig. 1 e), i.e., the amount of emission reduction necessary to comply with the 1.5°C climate target on a 1000-year timescale.

In the third approach, *A3*, oceanic CCS starts in year 2031 (Fig. 1 a) as the atmospheric CO_2 concentration caused by the RCP 4.5 CO_2 emission scenario starts to exceed the targeted RCP 2.6 atmospheric CO_2 concentration. Relative to preindustrial, global mean temperature continues to increase to a maximum of approximately +1.5°C in the year 2078 at a corresponding atmospheric CO_2 concentration of 433 ppmv (Figs. 1 b, c). Subsequently, temperature decreases until it reaches about +0.9 °C relative to preindustrial temperature, while the atmospheric CO_2 concentration reaches 327 ppmv at the end of the simulation (Figs. 1 b, c). Up to that point in time, cumulative CO_2 injections in the *A3* simulation amount to about 2200 Gt C (Fig. 1 a). In response to negative emissions the land turns into an atmospheric carbon source (Keller et al., 2018) between year 2076 and 2600 with a total loss of about 144 Gt C to the atmosphere. From year 2600 onwards, the carbon flux between the atmosphere and land is nearly zero (below 0.03 Gt C/yr^{-1}). By the end of the simulation, the diagnosed leakage of injected carbon adds up to about 900 Gt C (Fig. 1 d), which means that about 59 % of the injected CO_2 that remains in the ocean until year 3020. The required emission reduction to move from an RCP4.5 pathway to RCP 2.6 in the *A3* run is about 1300 Gt C (Fig. 1 e).

By the end of the *A3* simulation, cumulative CO_2 injections are about 636 Gt C (29 %) higher than in the *A2* simulation. This is also reflected in the higher diagnosed leakage by about 293 Gt C in total, when compared to the *A2* simulation. In the attempt to follow the atmospheric CO_2 concentration of the RCP2.6 (section 2.3), cumulative CO_2 injections are almost twice the amount of the cumulative CO_2 emissions difference between the RCP4.5 scenario and the RCP2.6 scenario applied here. This can be explained by the fact that deep oceanic CCS steepens the surface to deep DIC-gradient (Fig. S3 a) fostering a back transport to the surface ocean. Most of this enhanced deep water DIC is transported with the meridional overturning circulation to the Southern Ocean (south of 40°S), where the largest fraction of the total leakage occurs in our injection experiments (Fig. S3 b). By the end of the *A1* simulation, we find that about 60 % of the diagnosed leakage has outgassed in the Southern Ocean compared to about 77 % in *A2* run and about 80 % in the *A3* simulation. Overall, we find that, the higher the direct CO_2 injections into the deep ocean are, the higher the leakage (Figs. 1 a, d) and the higher the relative portion outgassed in the Southern Ocean.

What this means in terms of the effectiveness of oceanic CCS is further highlighted by the comparison of the required cumulative CO_2 injections of the three different approaches (*A1, A2*, and *A3*) and the respective required emission reductions needed to reach the run's specific climate target under a RCP/ECP 4.5 CO_2 emission scenario. As illustrated in Figs. 2 a, b, c, the approaches *A1*, *A2* and *A3* represent increasingly stringent climate targets as evident from decreasing atmospheric warming relative to preindustrial conditions. Cumulative CO_2 injections by the year 2100 are largely equivalent to the required emission reduction, because only a tiny fraction of injected CO_2 has outgassed until that point in time (Figs. 1 d, 2 a). However, by the end of the millennial injection experiments, cumulative CO_2 injections are much larger than the required emission reductions in year 3020 as indicated by the slopes of the eye-fitted lines in Figs. 2 b, c. This is due to the fact that the leakage in the injection experiments (Fig. 1 d) requires a larger CO_2 removal effort, i.e., CO_2 that leaks out has to be

reinjected. If there were no leakage of injected carbon, i.e., perfect storage, then the cumulative CO_2 injections would equal the required emission reductions.

3.2 Sensitivities to $CaCO_3$ sediment feedbacks and weathering fluxes

As illustrated in Fig. 2 b, cumulative CO_2 injections in the *A2*$_{sed}$ simulation are about 165 Gt C (11 %) smaller until the year 3020 when compared to the *A2* run (1562 Gt C). This smaller CO_2 injection is a result of two processes ($CaCO_3$ sediment dissolution and constant terrestrial weathering), which both have the net effect of adding alkalinity to the model ocean, when compared to the standard experiments without sediment feedbacks and continuous weathering fluxes. By the end of the simulation, average ocean alkalinity has increased by 32 mmol/m^3 in the *A2*$_{sed}$ run compared to an average value of 2422 mmol/m^3 in the *A2* run. About 84 % of this increase in global mean alkalinity can be attributed to ocean CCS and resulting sediment dissolution at depth, the rest is from ocean acidification-induced $CaCO_3$ dissolution according to the RCP 4.5 CO_2-emission scenario, as evident from the control run with sediment and weathering feedback. An increase in ocean alkalinity may enhance the oceanic uptake of atmospheric CO_2, however, only if waters with increased alkalinity arrive at the surface waters and lower surface-ocean pCO_2. This, in turn, reduces the required CO_2 injections to reach and maintain the 1.5°C climate target. Dissolution of $CaCO_3$ deep-sea sediments caused by the injection of CO_2 into the deep ocean at 3000m causes the dissolution of 11.8 Pmol $CaCO_3$ in the *A2*$_{sed}$ simulation by year 3020 releasing 11.8 Pmol DIC and 23.6 Pmol alkalinity to the deep ocean. Highest $CaCO_3$ dissolution rates occur in the vicinity of the seven injection sites (Figs. S4 a, b). Hence, ocean acidification reaching the deep ocean and ocean CCS convert sediments from a $CaCO_3$ sink (116 Gt $CaCO_3$-C at the end of the respective spin-up run) to a source of its dissolution products. A second process that contributes to the increase in ocean alkalinity is the terrestrial $CaCO_3$ weathering flux which arrives in the surface ocean via river discharge, and amounts to about 19.3 Pmol alkalinity and 9.7 Pmol C (116 Gt C) by the end of the *A2*$_{sed}$ simulation.

Disentangling the relative role of the two processes (turning $CaCO_3$ burial into $CaCO_3$ dissolution; continuous flux of alkalinity from terrestrial weathering) with respect to stabilizing oceanic CO_2 uptake and thereby affecting the required CO_2 injections is not trivial. Waters affected by $CaCO_3$ sediment dissolution in the deep ocean need to return to the ocean surface before having an effect on surface ocean pCO_2 and oceanic CO_2 uptake (Cao et al., 2009). The fluxes from terrestrial weathering, however, are in our simulation, continuous and constant with time (no sensitivity of weathering to changes in atmospheric pCO_2, surface air temperature, precipitation, or terrestrial production), and directly arrive in the surface ocean via river inflow. It is thus likely that, in comparison to the standard experiments without terrestrial weathering, the latter affects the atmosphere-ocean CO_2-flux well before the alkalinity input related to $CaCO_3$ dissolution. Quantifying the effect of each process to reduce the required CO_2 injection individually, however, would require additional simulations, e.g. experiments with $CaCO_3$ dissolution turned on but terrestrial weathering turned off. This is beyond the scope of this study. In con-

sequence, of the two processes mentioned above, the required emission reduction amounts to about 846 Gt C, i.e. ~ 109 Gt C (11 %) less when compared to the *A2* run (Fig. 2 b).

The net effects of sediment/weathering feedbacks on the required CO_2 injections in simulations of the second approach described above are as well represented in the injection experiments of the first and third approach, but are of smaller magnitude, i.e., 5 % less (Fig. 2 a, b, c).

3.3 Biogeochemical impacts

Here, we present injection related biogeochemical impacts with respect to changes in pH and the saturation state of aragonite in the default simulations of the second (*A2*) and third approach (*A3*) and of the respective RCP 4.5 control run. Simulations of the first approach are neglected here, because this one cannot reach and maintain the 1.5°C climate target.

At the beginning of our default simulations (year 2020), the uptake of anthropogenic CO_2 has lowered average pH at the ocean surface by about 0.12 units, relative to its preindustrial value of about 8.16 (Fig. 3 a). This trend continues in the control simulation until its maximum reduction of about -0.25 units in the year 2762, which stays nearly constant until the end of the simulation (Fig. 3 a).

As direct CO_2 injections lead to a decline in the atmospheric CO_2 concentration (Fig. 1 c) and, in consequence, to a lower upper-ocean carbon uptake via air-sea gas exchange, we find smaller reductions in average ocean surface pH, i.e. reduced upper ocean acidification, after year 2045 in the *A2* simulation and after year 2031 in the *A3* run (Fig. 3 a), i.e., shortly after their respective starting points of oceanic CCS (Fig. 1 a). In year 3020 the average ocean surface pH in the *A2* simulation is about +0.13 units higher, when compared to the control run (Fig. 3 a). Using global mean surface ocean pH as a metric, surface ocean acidification in year 3020 compared to year 2020 is slightly more intense in the *A2* simulation, but even more reduced in the *A3* run. In both cases this is a direct effect of a lower atmospheric pCO_2 (Fig. 1 c) compared to year 2020. Amelioration of surface ocean pH shows regional variability (Fig. 3 b), with local maxima of the pH difference between the *A2* simulation and the control run in the year 3020 up to +0.23 units, in particular in northern latitudes (Fig. 3 b). However, surface ocean acidification is less reduced in the Southern Ocean and even slightly higher in parts of the Weddell Sea, where most of the injected CO_2 leaks back into the atmosphere (Fig. 3 b).

The simulated ameliorations in the surface ocean pH come at the expense of strongly acidified water masses in the vicinity of the seven injection sites at 3000m depth, when compared to the RCP 4.5 control run. In order to assess how much of the global ocean volume (~ 1.6×10^9 km^3) shifts to biotically critical pH values in our simulations, we define two pH categories. The first category is defined as $7.4 \leq pH \leq 7.8$ (solid lines in Fig. 3 c) and is chosen because studies have shown that all calcifiers such as coralline algae and foraminaferans are strongly reduced or are absent from acidified areas ($pH < 7.8$) and the overall biomass of the benthic community is about 30 % less compared to normal conditions (e.g., IPCC, 2011; Fabricius et al., 2015). The second category includes pH values that are lower than 7.4 (dashed lines in Fig. 3 c). Such low pH

values are for instance found in the vicinity of volcanic CO_2 vents and cause a massive drop in biodiversity (e.g., Ogden, 2013).

In our control simulation, we find a steady increase in the ocean volume characterized by $7.4 \leq pH \leq 7.8$, from about 11 % of total ocean volume in year 2020 to about 63 % in year 3020 (Fig. 3 c). Oceanic CCS in the *A2* and *A3* simulation leads to a much steeper increase of 'moderately' acidified waters ($7.4 \leq pH \leq 7.8$) with maximum values of 76 % and 71 %, respectively, in year 2551 (Fig. 3 c), but decreasing to 72 % and 64 % in year 3020. Considering our chosen category ($7.4 \leq pH \leq 7.8$) ocean CCS mainly speeds up interior-ocean acidification but does not increase the acidified volume at the end of the simulation very much. At the end of the simulation the *A3* simulation and the *A2* run show an increase of affected interior-ocean water by 1 and 13 %, respectively, compared to the control run.

Respective volumes of the second category ($pH < 7.4$) start to appear around the year 2400 in the control simulation and then slowly increase to about 2 % until the end of the simulation (Fig. 3 e). In contrast, oceanic CCS directly results in the immediate appearance of waters with $pH < 7.4$, with a volume steadily increasing until the year 3020 where it reaches 9 % of total ocean volume in the *A2* simulation and 15 % in the *A3* run (Fig 3 c). The differences in both pH categories between the injection experiments are due to the higher cumulative mass of injected CO_2 in the *A3* run, leading to a smaller volume in the first category and to a bigger volume in the second one (Figs. 1 a, 2 b).

In order to further identify extreme pH related to the injections, we look at minimum pH values. These are found at 3000m depth, i.e., the depth at which oceanic CCS is carried out. Relative to preindustrial conditions, the highest reductions in pH minima are found in the *A2* simulation with about -2.37 units in year 2062, however with large regional variability (Fig. 3 d, e). Subsequently, the pH minima in the *A2* simulation show strong oscillations until about the year 2400, which are caused by the different annual CO_2 injection rates. By the end of the *A2* simulation, minimum pH values at 3000m depth are up to 1 unit lower than in the control run (Fig. 3 d). We find a similar pattern in the *A3* simulation, although the pH reductions show only slight oscillations, resulting in a more constant pH reduction than in the *A2* simulation (Fig. 3 d). In comparison to the injection experiments, minimum pH values in the control run start to appear from the year 2300 onwards, leading to a reduction by about -0.17 units in the year 3020 (Fig. 3 d), i.e. the deep ocean feels ocean acidification very slowly.

To summarize we observe an increasing benefit in reduced acidification at the ocean surface with higher cumulative CO_2 injections, which comes at the expense of increasing acidified water masses in the intermediate and deep ocean with strongest pH reductions in the vicinity of the injection sites (Fig. 3 e). Figure 4 a, b illustrates this trade-off for the injection experiments of the *A2* and *A3* simulations as well as for the respective control runs in year 3020. By comparing the different simulations with each other, we find that continental weathering and $CaCO_3$ sediment feedbacks lead to a slightly higher increase in average pH at the ocean surface as well as smaller minimum pH values at 3000m depth, when compared to preindustrial. This is caused by the dissolution of $CaCO_3$ sediments and the terrestrial weathering flux, which both have the net effect of adding alkalinity to the ocean and thereby increasing the buffer capacity of seawater.

The reported reductions in global average surface pH in our control simulation caused by the partial oceanic uptake of the RCP 4.5 CO_2 emissions correspond to an increase in hydrogen ions (H^+), which partly react with carbonate ions (CO_3^{2-}) to form bicarbonate ions (HCO_3^-). This leads in consequence to a reduction in the surface saturation state (Ω) with respect to the $CaCO_3$ minerals aragonite and calcite. This is of importance to marine calcifiers, because the formation of shells and skeletons generally occurs where $\Omega > 1$ and dissolution occurs where $\Omega < 1$ (unless the shells or skeletons are protected, for instance, by organic coatings) (Doney et al., 2009; Guinotte and Fabry, 2008). Since aragonite is about 1.5 times more soluble than calcite (Mucci, 1983) and since aragonite is the mineral form of coral reefs, which are of large socio-economic value, we only report here on simulated changes in the saturation state of aragonite.

To investigate how tropical coral reef habitats might be impacted in our simulations, we here define the potential coral reef habitat as the volume of the global upper ocean (0:130 m, the two topmost model grid cells), which is characterized by $\Omega_{AR} > 3.4$ and ocean temperatures between 21°C and 28°C, where most coral reefs exist (Kleypas et al., 1999). We present this volume as the percent fraction of the total upper ocean volume (4.637×10^7 km^3) in our model.

For preindustrial conditions (year 1765), we find that about 37 % of the upper ocean volume is within our defined thresholds (green star in Figs. 5 a, b). At the beginning of our simulations (year 2020), this coral reef habitat volume has already declined to about 13 %, consistent with the current observation that many coral reefs are already under severe stress (e.g., Pandolfi et al., 2011; Ricke et al., 2013). In the RCP 4.5 control run, we observe that the potential tropical coral reef habitat volume reaches 0 % in the year 2056 and remains so thereafter (Fig. 5 a) with a decrease in aragonite oversaturation levels being the main driver.

In our injection experiments, we find an increase in the potential tropical coral reef habitat volume right after the start of oceanic CCS (Fig. 5 a). Despite this, in the *A2* simulation the respective volume still approaches zero (0.2 %) in the year 2044, although it does then steadily increase again until it reaches 21 % at the end of the simulation, i.e. still 16 % less than its preindustrial state, but also 8% more compared to the current situation (Figs. 5 a, b). The respective habitat volume in the *A3* simulation shows an earlier and stronger increase, resulting in a habitat volume of about 34 %, i.e. 3 % less than preindustrial, at the end of the model experiment (Fig. 5 a).

In preindustrial times, water masses in the upper ocean (0 - 130 m) that were undersaturated with respect to aragonite ($\Omega_{AR} < 1$) were negligible (0.2 %; Fig. 5 c, green star). This undersaturated volume has increased to about 1 % at the beginning of our simulations. Over the course of the control run, we observe an increase with a maximum of about 9 % in the year 2212. Subsequently, the respective undersaturated volume slightly decreases until it reaches a minimum of about 7 % at the end of the simulation. Undersaturated surface waters are located in higher latitudes (Fig. 5 d), which is for instance considered a threat to pteropods like Limacina helicina (e.g., Lischka et al., 2011). In the *A2* and *A3* simulations, the respective undersaturated volumes are significantly smaller and never exceed 2 % of the surface ocean volume (Fig 5 c, d). Undersaturated surface-water volumes in the *A2* run are slightly higher than those in the *A3* simulation.

Further, we assess the volume that is undersaturated with respect to aragonite in the intermediate and deep ocean (130 - 6080 m) and present it as a %-fraction of the entire interior ocean volume (1.311x 10^9 km^3). This is of interest since changes in interior-ocean Ω_{AR} may affect the growth conditions of cold-water corals (e.g., Guinotte et al., 2008; Flögel et al., 2014; Roberts and Cairns, 2014) and the dissolution depth of sinking aragonite particles.

At the beginning of the simulations, 69 % of the interior oceans are undersaturated with respect to aragonite, which is about 3 % more than preindustrial (Fig. 5 e). Subsequently, the increase in undersaturated water volume is similar among all simulations until about the year 2122, when the undersaturated volume in the control simulation continues to increase until its maximum of about 91 % in the year 2713. The undersaturated volumes in the injection experiments show only a very small increase after year 2122, leading until year 3020 to values of about 86 % in both injection simulations (Fig. 5 e). The bigger volume in the control run is likely caused by acidified waters at the ocean surface that ventilate intermediate and mode waters (Resplandy et al., 2013).

Figs. 6 a, b shows a similar trade-off in the injection experiments of the second and third approach in year 3020 as for pH (Figs. 4 a, b), i.e. an increase of the aragonite saturation states in the upper ocean and an increase of undersaturated conditions in the intermediate and deep ocean. Further, the effects of $CaCO_3$ sediment dissolution and continental weathering lead to the highest benefit in the upper ocean and the lowest harm in the intermediate and deep ocean (Figs. 6 a, b).

As mentioned in the introduction, the neglect of non-CO_2 greenhouse gases in our injection experiments underestimates the required cumulative CO_2 injections and associated trade-offs in each approach. This is due to the fact that non-CO_2 greenhouse gases directly affect the Earth's energy balance, resulting in either warming or cooling of the atmosphere. Gases like methane and nitrous oxide warm the Earth, while aerosols such as sulfate cool it (e.g., Myhre et al., 2013). The current net effect is a small positive radiative forcing, which, although controversially debated, is expected to increase as the cooling effect of sulfate aerosols is predicted to decline over the next half of this century (Moss et al., 2010; Hansen et al., 2017; Rao et al., 2017).

4. Conclusion

This modeling study explores the potential and biogeochemical impacts of three different approaches to control the amount of oceanic CCS as a means to fill the gap between the CO_2 emissions and climate impacts of the RCP 4.5 scenario and a specific temperature target such as the 1.5°C climate target. We do so from the perspective of using only ocean CCS for this purpose.

The analysis of the *A1* simulation (first approach) reveals that because of committed warming and eventually outgassing of some of the injected CO_2, it would not be sufficient to inject the residual of the RCP 4.5 CO_2 emissions (964 Gt C in total) until the year 3020 once a global mean temperature of 1.5°C is exceeded for the first time (year 2045). In order to overcome the observed overshoot of +0.7°C by year 3020 in the first approach, we find that about 600 Gt C (62 %) more

need to be injected, as indicated by the default simulation of the second approach, i.e., *A2* run (Figs. 1 a, b, 2 b).

To follow the atmospheric CO_2 concentration of the RCP/ECP 2.6 as closely as possible by applying oceanic CCS would require cumulative CO_2 injections of about 2200 Gt C until the year 3020. However, global mean temperature reaches +0.9°C by the end of the *A3* simulation and thus undershoots the respective climate target.

The cumulative CO_2 injections in the second and third approach and the respective required emission reductions questions the suitability of oceanic CCS for the aspired target on such a timescale, because the outgassed CO_2 amounts, which are 607 and 900 Gt C by year 3020, respectively (Figs. 1 d, 2 b, c), would need to be re-captured by additional technologies such as Direct Air Capture and subsequently re-injected into the deep ocean. The required emission reductions of about 955 Gt C in the second and about 1300 Gt C in the third approach, point to the massive CO_2 amounts that would need to get removed from the atmosphere under the RCP/ECP 4.5 CO_2 emission scenario in order to be compatible with the 1.5°C or lower climate target on a millennium timescale.

From the integrated analysis of the model runs from all three approaches (i.e. eye-fitted lines in Figs. 2 b, c), we quantify the amount of emission reduction and oceanic CCS, respectively, required to lower the model-predicted global mean temperature by 1°C. In the near-term (2100) this measure is 446 Gt C / 1°C for both oceanic CCS and the required emission reductions as only a tiny fraction has outgassed until that point in time (see section 3.1). On a millennial timescale this measure is about 951 Gt C / 1°C for oceanic CCS and about 595 Gt C / 1°C (37 % less) for the required emission reductions, respectively, highlighting that a large fraction of injected CO_2 has outgassed.

Inclusion of $CaCO_3$ sediment and weathering feedbacks reduces the required cumulative CO_2 injections and required emission reductions by about 6 % in the first and third approach and by about 11 % in the second approach, respectively (Fig. 2 b, c). The neglect of non-CO_2 greenhouse gases in the applied forcing of the injection experiments underestimates the cumulative CO_2 injections that would be required. In general, it is estimated that non-CO_2 climate agents contribute between 10-30 % of the total forcing (Friedlingstein et al., 2014) until the year 2100 and for business-as-usual simulations. Extrapolating the current contribution of greenhouse gases other than CO_2 qualitatively into the future we expect that CO_2-injections of the magnitude of the *A3* simulation may be required to stay safely below +1.5°C on a millennium timescale. We propose, that our generalized estimates of emission reduction and oceanic CCS per 1°C cooling, respectively, may be used in the future to quantify additional efforts in order to compensate for non-CO_2 greenhouse gases induced warming.

With respect to the biogeochemical impacts in the injection simulations of the second and third approach, we observe an increase of average pH and aragonite saturation states in the surface ocean (0 - 130 m) after the start of oceanic CCS, when compared to the RCP 4.5 control run. These are due to the direct effect of a lower atmospheric pCO_2 in the injection experiments, i.e., reduced upper ocean acidification (section 3.3).

Potential tropical coral reef habitats in the upper ocean volume, which are here defined as $\Omega_{AR} > 3.4$ and ocean temperatures between 21°C and 28°C, are observed to steadily increase after the start of oceanic CCS in the *A2* run and the

A3 simulation (Fig. 5 a), almost reaching preindustrial levels in the *A3* simulation. However, the potential coral reef habitats in the respective injection experiments are close to zero for several decades (Fig. 5 a), raising the question if coral reefs would be able to recover from globally inhabitable conditions after this period of time. Local application of ocean alkalinization (Feng et al., 2016) may be a technical solution to protect coral reefs during this time period, in particular in regions where coral reefs are essential for shoreline protections.

The observed reduction of ocean acidification in the surface ocean comes at the expense of more strongly acidified water masses in the intermediate and deep ocean, with strongest reductions in pH in the vicinity of the seven injections sites (Figs. 3 d, e). Although it is difficult to predict how this would impact marine ecosystems, it is very likely that such conditions would put them under severe stress.

Overall, the trade-off between injection-related damages in the deep ocean and benefits in the upper ocean illustrate the challenge of evaluating the offset of local harm against global benefit, which is very likely the subject of any deliberate CO_2 removal method (e.g., Smith et al., 2016; Boysen et al., 2017; Fuss et al., 2018). Leaving aside the massive economic effort associated with ocean CCS of the size needed to reach the 1.5°C climate target (even when starting from a currently optimistic RCP 4.5 mitigation scenario), humanity will have to decide whether severe stress and potential loss of deep-sea ecosystems is acceptable when paid off by conserving or restoring surface ocean ecosystems to a large extent.

Data availability

The model data used to generate the table and figures is available online at https://data.geomar.de/thredds/catalog/open_access/reith_et_al_2019_esd/catalog.html

Author contributions

All authors conceived and designed the experiments. FR implemented the experiments with contributions from WK and JG. FR performed the experiments and analysed the data. FR wrote the manuscript with contributions from all co-authors.

Competing interests

The authors declare that they have no conflict of interest.

Acknowledgments

The Deutsche Forschungsgemeinschaft (DFG) financially supported this study via the Priority Program 1689.

References

Allen, M. R., Frame, D. J., Huntingford, C., Jones, C. D., Lowe, J. A., Meinshausen, M. and Meinshausen, N.: Warming caused by cumulative carbon emissions towards the trillionth tonne, Nature, 458(7242), 1163–1166, doi:10.1038/nature08019, 2009.

Archer, D.: A data-driven model of the global calcite lysocline, Global Biogeochem. Cycles, 10(3), 511–526, doi:10.1029/96GB01521, 1996.

Archer, D.: Fate of fossil fuel CO_2 in geologic time, J. Geophys. Res. C Ocean., 110(9), 1–6, doi:10.1029/2004JC002625, 2005.

Archer, D., Kheshgi, H. S. and Maier-Reimer, E.: Dynamics of fossil fuel CO_2 neutralization by marine $CaCO_3$, Glob. Biogeochem. Cycles, 12(2), 259–276, 1998.

Bigalke, N. K., Rehder, G. and Gust, G.: Experimental investigation of the rising behavior of CO_2 droplets in seawater under hydrate-forming conditions, Environ. Sci. Technol., 42(14), 5241–5246, doi:10.1021/es800228j, 2008.

Bitz, C. M. and Lipscomb, W. H.: An energy-conserving thermodynamic model of sea ice, J. Geophys. Res., 104(C7), 15669, doi:10.1029/1999JC900100, 1999.

Boysen, L., Lucht, W., Schellnhuber, H., Gerten, D., Heck, V. and Lenton, T.: The limits to global-warming mitigation by terrestrial carbon removal, Earth' s Future, 5(5), 1–12, doi:10.1002/eft2.203, 2017.

Cao, L., Eby, M., Ridgwell, A., Caldeira, K., Archer, D., Ishida, A., Joos, F., Matsumoto, K., Mikolajewicz, U., Mouchet, A., Orr, J. C., Plattner, G.-K., Schlitzer, R., Tokos, K., Totterdell, I., Tschumi, T., Yamanaka, Y. and Yool, A.: The role of ocean transport in the uptake of anthropogenic CO_2, Biogeosciences, 6(3), 375–390, doi:10.5194/bg-6-375-2009, 2009.

Clarke, L. E., Jiang, K., Akimoto, K., Babiker, M., Blanford, G., Fisher-Vanden, K., Hourcade, J.-C., Krey, V., Kriegler, E., Löschel, A., McCollum, D., Paltsev, S., Rose, S., Shukla, P. R., Tavoni, M., van der Zwaan, B. C. C. and van Vuuren, D. P.: Assessing transformation pathways, Clim. Chang. 2014 Mitig. Clim. Chang. Contrib. Work. Gr. III to Fifth Assess. Rep. Intergov. Panel Clim. Chang., 413–510, 2014.

Clémençon, R.: The Two Sides of the Paris Climate Agreement, J. Environ. Dev., 25(1), 3–24, doi:10.1177/1070496516631362, 2016.

Collins, M., Knutti, R., Arblaster, J., Dufresne, J.-L., Fichefet, T., Friedlingstein, P., Gao, X., Gutowski, W. J., Johns, T., Krinner, G., Shongwe, M., Tebaldi, C., Weaver, A. J. and Wehner, M.: Long-term Climate Change: Projections, Commitments and Irreversibility, Clim. Chang. 2013 Phys. Sci. Basis. Contrib. Work. Gr. I to Fifth Assess. Rep. Intergov. Panel Clim. Chang., 1029–1136, doi:10.1017/CBO9781107415324.024, 2013.

DeVries, T. and Primeau, F.: Dynamically and Observationally Constrained Estimates of Water-Mass Distributions and Ages in the Global Ocean, J. Phys. Oceanogr., 41(12), 2381–2401, doi:10.1175/JPO-D-10-05011.1, 2011.

Dickson, A. G. and Millero, F. J.: A comparison of the equilibrium constants for the dissociation of carbonic acid in seawater media, Deep Sea Res. Part A, Oceanogr. Res. Pap., 34(10), 1733–1743, doi:10.1016/0198-0149(87)90021-5, 1987.

Doney, S. C., Fabry, V. J., Feely, R. a and Kleypas, J. a: Ocean acidification: the other CO_2 problem., Ann. Rev. Mar. Sci., 1, 169–92, doi:10.1146/annurev.marine.010908.163834, 2009.

Fabricius, K. E., Kluibenschedl, A., Harrington, L., Noonan, S. and De'ath, G.: In situ changes of tropical crustose coralline algae along carbon dioxide gradients, Sci. Rep., 5, 9537, doi:10.1038/srep09537, 2015.

Fanning, A. F. and Weaver, A. J.: An atmospheric energy-moisture balance model: Climatology, interpentadal climate change, and coupling to an ocean general circulation model, J. Geophys. Res., 101(D10), 15111, doi:10.1029/96JD01017, 1996.

Feng, E. Y., Keller, D. P., Koeve, W. and Oschlies, A.: Could artificial ocean alkalinization protect tropical coral ecosystems from ocean acidification?, Environ. Res. Lett., 11(7), 74008, doi:10.1088/1748-9326/11/7/074008, 2016.

Field, C., Barros, V., Stocker, T. and Dahe, Q.: IPCC workshop on impacts of ocean acidification on marine biology and ecosystems. Workshop report. [online] Available from: https://www.etde.org/etdeweb/details_open.jsp?osti_id=1032894, 2011.

Flögel, S., Dullo, W. C., Pfannkuche, O., Kiriakoulakis, K. and Rüggeberg, A.: Geochemical and physical constraints for the occurrence of living cold-water corals, Deep. Res. Part II Top. Stud. Oceanogr., 99, 19–26, doi:10.1016/j.dsr2.2013.06.006, 2014.

Friedlingstein, P., Andrew, R. M., Rogelj, J., Peters, G. P., Canadell, J. G., Knutti, R., Luderer, G., Raupach, M. R., Schaeffer, M., Vuuren, D. P. Van and Quéré, C. Le: Persistent growth of CO_2 emissions and implications for reaching climate targets, Nat. Publ. Gr., 7(10), 709–715, doi:10.1038/ngeo2248, 2014.

Fuss, S., Canadell, J. G., Peters, G. P., Tavoni, M., Andrew, R. M., Ciais, P., Jackson, R. B., Jones, C. D., Kraxner, F., Nakicenovic, N., Le Quere, C., Raupach, M. R., Sharifi, A., Smith, P., Yamagata, Y., Le Quéré, C., Raupach, M. R., Sharifi, A., Smith, P. and Yamagata, Y.: Betting on negative emissions, Nat. Clim. Chang., 4(10), 850–853, doi:10.1038/nclimate2392, 2014.

Fuss, S., Lamb, W. F., Callaghan, M. W., Hilaire, J., Creutzig, F., Amann, T., Beringer, T., De Oliveira Garcia, W., Hartmann, J., Khanna, T., Luderer, G., Nemet, G. F., Rogelj, J., Smith, P., Vicente, J. V., Wilcox, J., Del Mar Zamora Dominguez, M. and Minx, J. C.: Negative emissions - Part 2: Costs, potentials and side effects, Environ. Res. Lett., 13(6), doi:10.1088/1748-9326/aabf9f, 2018.

Gasser, T., Guivarch, C., Tachiiri, K., Jones, C. D. and Ciais, P.: Negative emissions physically needed to keep global warming below 2 °C, Nat. Commun., 6, 7958, doi:10.1038/ncomms8958, 2015.

Gehlen, M., Séférian, R., Jones, D. O. B., Roy, T., Roth, R., Barry, J., Bopp, L., Doney, S. C., Dunne, J. P., Heinze, C., Joos, F., Orr, J. C., Resplandy, L., Segschneider, J. and Tjiputra, J.: Projected pH reductions by 2100 might put deep North Atlantic biodiversity at risk, Biogeosciences, 11(23), 6955–6967, doi:10.5194/bg-11-6955-2014, 2014.

Gillett, N. P., Arora, V. K., Zickfeld, K., Marshall, S. J. and Merryfield, W. J.: Ongoing climate change following a complete cessation of carbon dioxide emissions, Nat. Geosci., 4(2), 83–87, doi:10.1038/ngeo1047, 2011.

Guinotte, J. M. and Fabry, V. J.: Ocean acidification and its potential effects on marine ecosystems, Ann. N. Y. Acad. Sci., 1134, 320–342, doi:10.1196/annals.1439.013, 2008.

Guinotte, J. M., Orr, J., Cairns, S., Freiwald, A., Morgan, L. and George, R.: Will human-induced changes in seawater chemistry alter the distribution of deep-sea scleractinian corals?, Front. Ecol. Environ., 4(3), 141–146, doi:10.1890/1540-9295(2006)004[0141:WHCISC]2.0.CO;2, 2006.

Hansen, J., Sato, M., Kharecha, P., Schuckmann, K. Von and Beerling, D. J.: Young people ' s burden : requirement of negative CO 2 emissions, , 577–616, 2017.

Hoffert, M. I., Wey, Y. C., Callegari, A. J. and Broecker, W. S.: Atmospheric response to deep-sea injections of fossil-fuel carbon dioxide, Clim. Change, 2(1), 53–68, doi:10.1007/BF00138226, 1979.

Horton, J. B., Keith, D. W. and Honegger, M.: Implications of the Paris Agreement for Carbon Dioxide Removal and Solar Geoengineering, , 1–10, 2016.

Intergovernmental Panel on Climate Change (IPCC), [Metz, B., Davidson, O., de Coninck, H. C., Loos, M., and Meyer, L. A. (eds.)]: Special Report on Carbon Dioxide Capture and Storage, Cambridge University Press, Cambridge, United Kingdom and New York, NY, USA, 422pp., 2005.

Intergovernmental Panel on Climate Change (IPCC): Workshop Report of the IPCC Workshop on Impacts of Ocean Acidification on Marine Biology and Ecosystems [Field, C.B., Barros, V., Stocker, T.F., Qin, D. , Mach, K.J., Plattner, G.-K., Mastrandrea, M.D., Tignor, M., and Ebi, K.L. (eds.)]. IPCC Working Group II Technical Support Unit, Carnegie Institution, Stanford, California, United States of America, pp. 164, 2011.

Jain, A. K. and Cao, L.: Assessing the effectiveness of direct injection for ocean carbon sequestration under the influence of climate change, Geophys. Res. Lett., 32, L09609, doi:10.1029/2005GL022818, 2005.

Keeling, R. F.: Triage in the greenhouse, Nat. Geosci., 2(12), 820–822, doi:10.1038/ngeo701, 2009.

Keller, D. P., Oschlies, a. and Eby, M.: A new marine ecosystem model for the University of Victoria Earth System Climate

Model, Geosci. Model Dev., 5(5), 1195–1220, doi:10.5194/gmd-5-1195-2012, 2012.

Keller, D. P., Feng, E. Y. and Oschlies, A.: Potential climate engineering effectiveness and side effects during a high carbon dioxide-emission scenario., Nat. Commun., 5, 3304, doi:10.1038/ncomms4304, 2014.

Keller, D. P., Lenton, A., Littleton, E. W., Oschlies, A., Scott, V. and Vaughan, N. E.: The Effects of Carbon Dioxide Removal on the Carbon Cycle, Curr. Clim. Chang. Reports, 4(3), 250–265, doi:10.1007/s40641-018-0104-3, 2018.

Kleypas, J. A., et al.: Environmental limits to coral reef development: Where do we draw the line?, Am. Zool., 39(1), 146–159, 1999.

Knopf, B., Fuss, S., Hansen, G., Creutzig, F., Minx, J. and Edenhofer, O.: From Targets to Action: Rolling up our Sleeves after Paris, Glob. Challenges, 1(2), 1600007, doi:10.1002/gch2.201600007, 2017.

Knutti, R., Rogelj, J., Sedláček, J. and Fischer, E. M.: A scientific critique of the two-degree climate change target, Nat. Geosci., 9(1), doi:10.1038/ngeo2595, 2015.

Koeve, W. and Oschlies, A.: Potential impact of DOM accumulation on fCO(2) and carbonate ion computations in ocean acidification experiments, Biogeosciences, 9(10), 3787–3798, doi:10.5194/bg-9-3787-2012, 2012.

Leung, D. Y. C., Caramanna, G. and Maroto-Valer, M. M.: An overview of current status of carbon dioxide capture and storage technologies, Renew. Sustain. Energy Rev., 39, 426–443, doi:10.1016/j.rser.2014.07.093, 2014.

Lewis, E. and Wallace, D.: Program developed for CO_2 system calculations, Ornl/Cdiac-105, 1–21, doi:4735, 1998.

Lischka, S., Büdenbender, J., Boxhammer, T. and Riebesell, U.: Impact of ocean acidification and elevated temperatures on early juveniles of the polar shelled pteropod Limacina helicina: Mortality, shell degradation, and shell growth, Biogeosciences, 8(4), 919–932, doi:10.5194/bg-8-919-2011, 2011.

MacDougall, A. H.: The Transient Response to Cumulative CO_2 Emissions: a Review, Curr. Clim. Chang. Reports, 2(1), 39–47, doi:10.1007/s40641-015-0030-6, 2016.

Marchetti, C.: On geoengineering and the CO_2 problem, Clim. Change, 1(1), 59–68, doi:10.1007/BF00162777, 1977.

Matthews, H. D. and Caldeira, K.: Stabilizing climate requires near-zero emissions, Geophys. Res. Lett., 35(4), 1–5, doi:10.1029/2007GL032388, 2008.

Matthews, H. D., Gillett, N. P., Stott, P. a and Zickfeld, K.: The proportionality of global warming to cumulative carbon emissions., Nature, 459(7248), 829–32, doi:10.1038/nature08047, 2009.

Mehrbach, C., Culberson, C. H., Hawley, J. E. and Pytkowicx, R. M.: Measurement of the Apparent Dissociation Constants of Carbonic Acid in Seawater At Atmospheric Pressure1, Limnol. Oceanogr., 18(6), 897–907, doi:10.4319/lo.1973.18.6.0897, 1973.

Meinshausen, M., Smith, S. J., Calvin, K., Daniel, J. S., Kainuma, M. L. T., Lamarque, J., Matsumoto, K., Montzka, S. a., Raper, S. C. B., Riahi, K., Thomson, a., Velders, G. J. M. and van Vuuren, D. P. P.: The RCP greenhouse gas concentrations and their extensions from 1765 to 2300, Clim. Change, 109(1), 213–241, doi:10.1007/s10584-011-0156-z, 2011.

Mengis, N., Partanen, A. I., Jalbert, J. And Matthews, H. D.: 1.5°C carbon budget dependent on carbon cycle uncertainty and future non-CO_2 forcing, Sci. Rep., 8(1), 1-7, doi:10.1038/s41598-018-24241-1, 2018.

Meissner, K. J., Weaver, a. J., Matthews, H. D. and Cox, P. M.: The role of land surface dynamics in glacial inception: A study with the UVic Earth System Model, Clim. Dyn., 21(7–8), 515–537, doi:10.1007/s00382-003-0352-2, 2003.

Moss, R. H., Edmonds, J. a, Hibbard, K. a, Manning, M. R., Rose, S. K., van Vuuren, D. P., Carter, T. R., Emori, S., Kainuma, M., Kram, T., Meehl, G. a, Mitchell, J. F. B., Nakicenovic, N., Riahi, K., Smith, S. J., Stouffer, R. J., Thomson, A. M., Weyant, J. P. and Wilbanks, T. J.: The next generation of scenarios for climate change research and assessment., Nature, 463(7282), 747–56, doi:10.1038/nature08823, 2010.

Mucci A.: The solubility of calcite and aragonite in seawater at various salinities, temperatures and one atmosphere total pressure. Amer. Jour. Sci. 283: 780-799, 1983.

Myhre, G., Samset, B. H., Schulz, M., Balkanski, Y., Bauer, S., Berntsen, T. K., Bian, H., Bellouin, N., Chin, M., Diehl, T.,

655 Easter, R. C., Feichter, J., Ghan, S. J., Hauglustaine, D., Iversen, T., Kinne, S., Kirkeväg, A., Lamarque, J. F., Lin, G., Liu, X., Lund, M. T., Luo, G., Ma, X., Van Noije, T., Penner, J. E., Rasch, P. J., Ruiz, A., Seland, Skeie, R. B., Stier, P., Takemura, T., Tsigaridis, K., Wang, P., Wang, Z., Xu, L., Yu, H., Yu, F., Yoon, J. H., Zhang, K., Zhang, H. and Zhou, C.: Radiative forcing of the direct aerosol effect from AeroCom Phase II simulations, Atmos. Chem. Phys., 13(4), 1853–1877, doi:10.5194/acp-13-1853-2013, 2013.

660 Ogden, L. E.: Marine Life on Acid, Bioscience, 63(5), 322–328, doi:10.1525/bio.2013.63.5.3, 2013.

Orr, J. C., Najjar, C. R., Sabine, C. L., and Joos, F.: Abiotic-Howto. Internal OCMIP Report, LCSE/CEA Saclay, Gif-sur-Yvette, France, 25pp, 1999.

Orr, J. C., Aumont, O., Yool, A., Plattner, K., Joos, F., Maier-Reimer, E., Weirig, M. -F., Schlitzer, R., Caldeira, K., Wicket, M., and Matear, R.: Ocean CO_2 Sequestration Efficiency from 3-D Ocean Model Comparison, in Greenhouse Gas Control Tech-

665 nologies), edited by Williams, D., Durie, B., McMullan, P., Paulson, C., and Smith, A., CSIRO, Colligwood, Australia, pp. 469-474, 2001.

Orr, J. C.: Modelling of ocean storage of CO_2 - The GOSAC study, Report PH4/37, IEA Greenhouse gas R&D Programme, 96pp., 2004.

Pacanowski, R. C.: MOM2: Documentation, User's Guide and Reference Manual, GFDL Ocean Tech. Rep., 3.2, 329pp, 1996.

670 Pandolfi, J. M., Connolly, S. R., Marshall, D. J. and Cohen, A. L.: Projecting Coral Reef Futures Under Global Warming and Ocean Acidification, Science (80-.)., 333(6041), 418–422, doi:10.1126/science.1204794, 2011.

Rao, S., Klimont, Z., Smith, S. J., Van Dingenen, R., Dentener, F.,Bouwman, L., Riahi, K., Amann, M., Bodirsky, B. L., van Vuuren, D. P., Reis, L. A., Calvin, K., Drouet, L., Fricko, O., Fujimori, S., Gernaat, D., Havlik, P., Harmsen, M., Hasegawa, T., Heyes, C., Hilaire, J., Luderer, G., Masui, T., Stehfest, E., Strefler, J., van der Sluis, S., and Tavoni, M.: Future air pollu-

675 tion in the Shared Socio-economic Pathways, Global Environ. Change, 42, 346–358, 2017.

Reith, F., Keller, D. P. and Oschlies, A.: Revisiting ocean carbon sequestration by direct injection: A global carbon budget perspective, Earth Syst. Dyn., 7(4), 797–812, doi:10.5194/esd-7-797-2016, 2016.

Resplandy, L., Bopp, L., Orr, J. C. and Dunne, J. P.: Role of mode and intermediate waters in future ocean acidification: Analysis of CMIP5 models, Geophys. Res. Lett., 40(January), 3091–3095, doi:10.1002/grl.50414, 2013.

680 Ricke, K. L., Orr, J. C., Schneider, K. and Caldeira, K.: Risks to coral reefs from ocean carbonate chemistry changes in recent earth system model projections, Environ. Res. Lett., 8(3), 34003, doi:10.1088/1748-9326/8/3/034003, 2013.

Ridgwell, A., Rodengen, T. J. and Kohfeld, K. E.: Geographical variations in the effectiveness and side effects of deep ocean carbon sequestration, Geophys. Res. Lett., 38(17), 1–6, doi:10.1029/2011GL048423, 2011.

Roberts, J. M. and Cairns, S. D.: Cold-water corals in a changing ocean, Curr. Opin. Environ. Sustain., 7, 118–126,

685 doi:10.1016/j.cosust.2014.01.004, 2014.

Rockström, J., Steffen, W., Noone, K., Persson, Å., Chapin III, F. S., Lambin, E. F., Lenton, T. M., Scheffer, M., Folke, C., Schellnhuber, H., Nykvist, B., de Wit, C. A., Hughes, T., van der Leeuw, S., Rodhe, H., Sörlin, S., Snyder, P. K., Costanza, R. and Al., E.: Planetary Boundaries: Exploring the Safe Operating Space for Humanity, Ecol. Soc., 14(2), 32, doi:10.1038/461472a, 2009.

690 Rockström, J., Schellnhuber, H., Hoskins, B., Ramanathan, V., Brasseur, G., Gaffney, O., Nobre, C., Meinshausen, M. and Lucht, W.: Earth ' s Future The world ' s biggest gamble Earth ' s Future, Earth's Futur., 4, 465–470, doi:10.1002/2016EF000392.Received, 2016.

Rogelj, J., Elzen, M. Den, Fransen, T., Fekete, H., Winkler, H., Schaeffer, R., Sha, F., Riahi, K. and Meinshausen, M.: Perspective : Paris Agreement climate proposals need boost to keep warming well below 2 ° C, Nat. Clim. Chang., 534(June),

695 doi:10.1038/nature18307, 2016.

Sabine, C. L., Feely, R. A., Gruber, N., Key, R. M., Lee, K., Bullister, J. L., Wanninkhof, R., Wong, C. S., Wallace, D. W. R., Tilbrook, B., Millero, F. J., Peng, T.-H., Kozyr, A., Ono, T. and Rios, A. F.: The oceanic sink for anthropogenic CO_2., Sci-

ence, 305(5682), 367–71, doi:10.1126/science.1097403, 2004.

Sanderson, B. M., O'Neill, B. C. and Tebaldi, C.: What would it take to achieve the Paris temperature targets?, Geophys. Res. Lett., 43(13), 7133–7142, doi:10.1002/2016GL069563, 2016.

Sarmiento, J. L. and Toggweiler, J. R.: A new model for the role of the oceans in determining atmospheric PCO_2, Nature, 308(5960), 621–624 [online] Available from: http://dx.doi.org/10.1038/308621a0, 1984.

Schubert, R., Schellnhuber, H. J., Buchmann, N., Epiney, A., Griesshammer, R., Kulessa, M., Messner, D., Rahmstorf, S. and Schmid, J.: The Future Oceans – Warming Up, Rising High, Turning Sour., 2006.

Smith, P., Davis, S. J., Creutzig, F., Fuss, S., Minx, J., Gabrielle, B., Kato, E., Jackson, R. B., Cowie, A., Kriegler, E., van Vuuren, D. P., Rogelj, J., Ciais, P., Milne, J., Canadell, J. G., McCollum, D., Peters, G., Andrew, R., Krey, V., Shrestha, G., Friedlingstein, P., Gasser, T., Grubler, A., Heidug, W. K., Jonas, M., Jones, C. D., Kraxner, F., Littleton, E., Lowe, J., Moreira, J. R., Nakicenovic, N., Obersteiner, M., Patwardhan, A., Rogner, M., Rubin, E., Sharifi, A., Torvanger, A., Yamagata, Y., Edmonds, J. and Yongsung, C.: Biophysical and economic limits to negative CO_2 emissions, Nat. Clim. Chang., 6(1), doi:10.1038/nclimate2870\rhttp://www.nature.com/nclimate/journal/v6/n1/abs/nclimate2870.html#supplementary-information, 2016.

UNFCCC. Conference of the Parties: Adoption of the Paris Agreement. Proposal by the President., Paris Clim. Chang. Conf. - Novemb. 2015, COP 21, 21932(December 2015), 31 [online] Available from: http://unfccc.int/resource/docs/2015/cop21/eng/l09.pdf, 2015.

van Heuven, S., Pierrot, D., Lewis, E., and Wallace, D. W.R.: MATLAB Program Developed for CO_2 System Calculations, ORNL/CDIAC-105b, Carbon Dioxide Information Analysis Center, Oak Ridge National Laboratory, US Department of Energy, Oak Ridge, Tennessee,

ftp://cdiac.ornl.gov/pub/co2sys/CO2SYScalcMATLAB, 2009.

Volk, T. and Hoffert, M. I.: Ocean carbon pumps: Analysis of relative strengths and efficiencies in ocean driven atmospheric CO_2 changes, in The Carbon Cycle and Atmospheric CO_2: Natural variations Archaean to present, ed. by Sundquist, E.T. and Broecker, W.S., Geophys. Monogr. Ser., 32, 99-110, AGU, Washington, D.C., 1985.

Weaver, A. J., Eby, M., Wiebe, E. C., Bitz, C. M., Duffy, P. B., Ewen, T. L., Fanning, A. F., Holland, M. M., MacFadyen, A., Matthews, H. D., Meissner, K. J., Saenko, O., Schmittner, A., Wang, H. and Yoshimori, M.: The UVic earth system climate model: Model description, climatology, and applications to past, present and future climates, Atmosphere-Ocean, 39(4), 361–428, doi:10.1080/07055900.2001.9649686, 2001.

Williamson, P.: Emissions reduction: Scrutinize CO_2 removal methods, Nature, 530(153), 5–7, doi:10.1038/530153a, 2016.

Zeebe, R. E.: History of Seawater Carbonate Chemistry, Atmospheric CO_2, and Ocean Acidification, Annu. Rev. Earth Planet. Sci., 40(1), 141–165, doi:10.1146/annurev-earth-042711-105521, 2012.

Zickfeld, K. and Herrington, T.: The time lag between a carbon dioxide emission and maximum warming increases with the size of the emission, Environ. Res. Lett., 10(3), 31001, doi:10.1088/1748-9326/10/3/031001, 2015.

Zickfeld, K., MacDougall, A. H. and Matthews, H. D.: On the proportionality between global temperature change and cumulative CO_2 emissions during periods of net negative CO_2 emissions, Environ. Res. Lett., 11(5), 55006, doi:10.1088/1748-9326/11/5/055006, 2016.

Earth Syst. Dynam. Discuss., https://doi.org/10.5194/esd-2018-87
Manuscript under review for journal Earth Syst. Dynam.
Discussion started: 1 March 2019

Earth System Dynamics Discussions Open Access EGU

Table 1: Overview of all conducted simulations and their set-up. The "X" denotes that the respective feature is applied. Note that the applied CO_2 forcing follows the RCP 4.5 CO_2 emission scenario from 2006-2100 and the Extended RCP 4.5 CO_2 emissions scenario from 2100-2500. From 2500 onwards CO_2 emissions linearly decline until zero Gt C yr^{-1} in year 3020.

	Set-up		
Simulation	CO_2 emissions forcing	$CaCO_3$ sediment and weathering feedbacks	Direct CO_2 injections at 3000 m depth
	2006-3020	2006-3020	2020-3020
RCP 4.5 control run	X		
A1	X		X
A1_Comitw	X		
A2	X		X
A3	X		X
RCP 4.5 $control_{sed}$ run	X	X	
$A1_{sed}$	X	X	X
$A1\_Comitw_{sed}$	X	X	
$A2_{sed}$	X	X	X
$A3_{sed}$	X	X	X

Earth Syst. Dynam. Discuss., https://doi.org/10.5194/esd-2018-87
Manuscript under review for journal Earth Syst. Dynam.
Discussion started: 1 March 2019

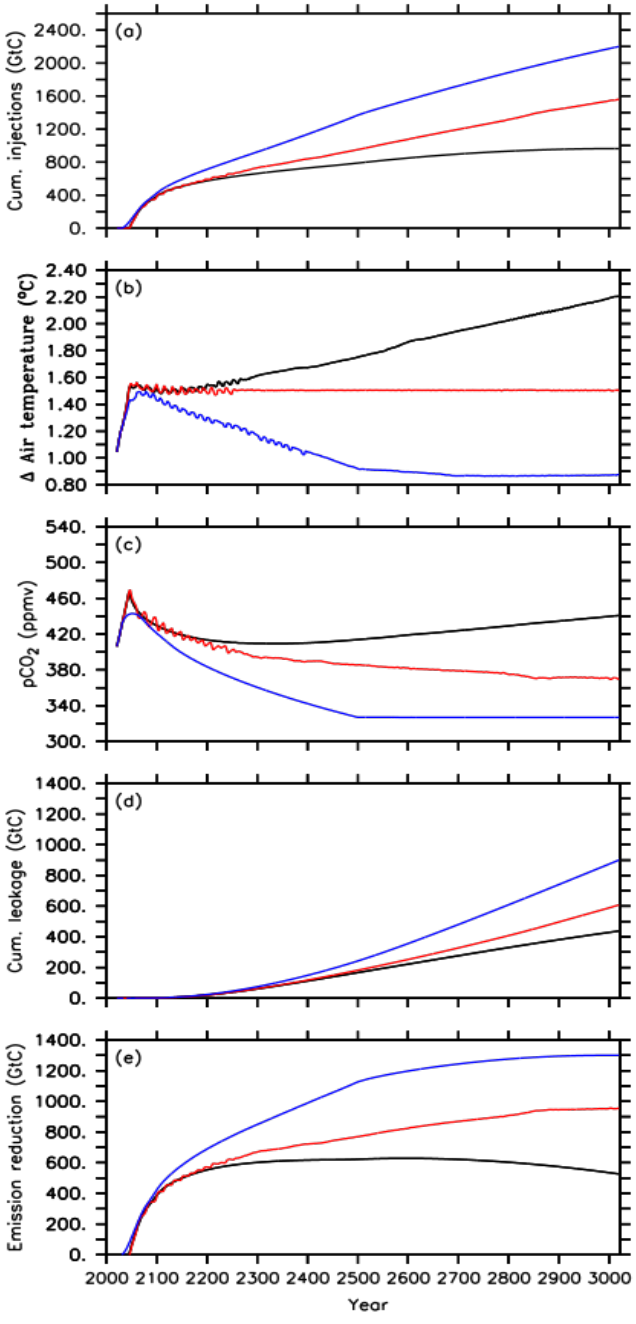

Figure 1: Time-series of the different default injection experiments, i.e., A1 simulation (black lines), A2 simulation (red lines) and A3 simulation (blue lines) for **(a)** cumulative CO_2 injections, **(b)** global mean surface air temperature, relative to preindustrial, **(c)** atmospheric CO_2 concentration, **(d)** cumulative leakage of injected CO_2, and **(e)** required emission reduction.

Earth Syst. Dynam. Discuss., https://doi.org/10.5194/esd-2018-87
Manuscript under review for journal Earth Syst. Dynam.
Discussion started: 1 March 2019

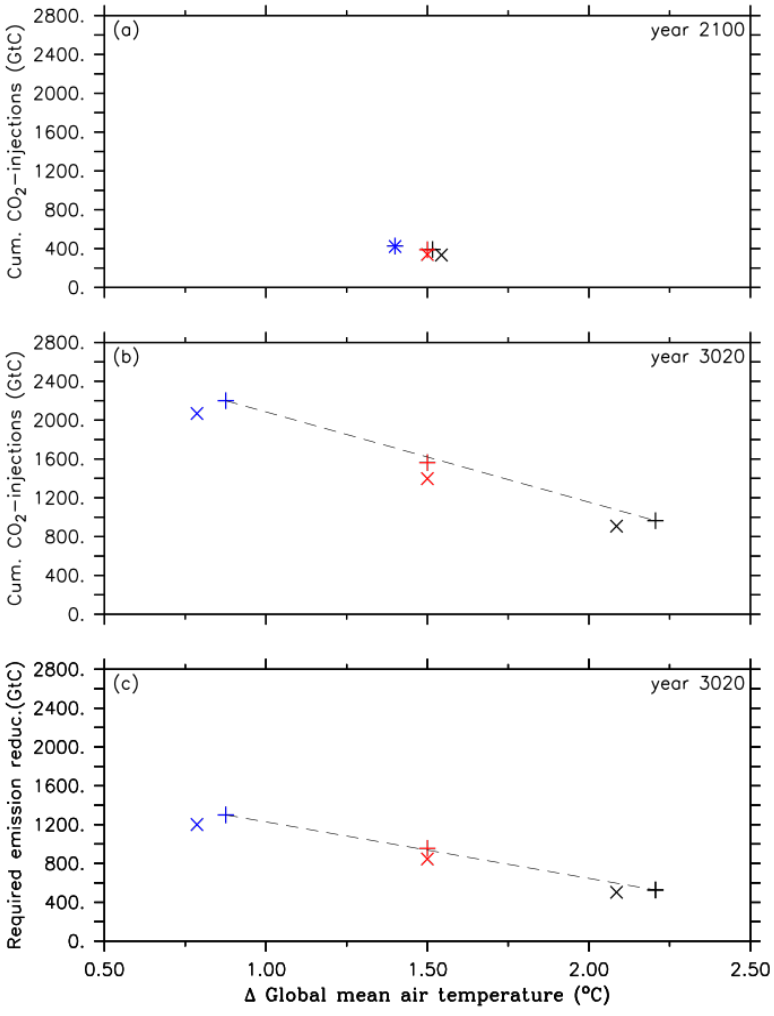

Figure 2: Comparison between simulations of the first approach (A1, black symbols), simulations of the second approach (A2, red symbols) and simulations of the third approach (A3, blue symbols). The cross symbols refer to the default simulations and the X symbols denote simulations with $CaCO_3$ sediment and weathering feedbacks. These symbols represent for **(a)** cumulative CO_2 injections and corresponding global mean temperature, relative to preindustrial, in year 2100 **(b)** cumulative CO_2 injections and corresponding global mean temperature, relative to preindustrial, at the end of the simulation (yr 3020), and **(c)** required emission reduction and corresponding global mean temperature, relative to preindustrial, at the end of the simulations. Note that the dashed black lines are eye-fitted to the results of the standard runs.

765

Earth Syst. Dynam. Discuss., https://doi.org/10.5194/esd-2018-87
Manuscript under review for journal Earth Syst. Dynam.
Discussion started: 1 March 2019

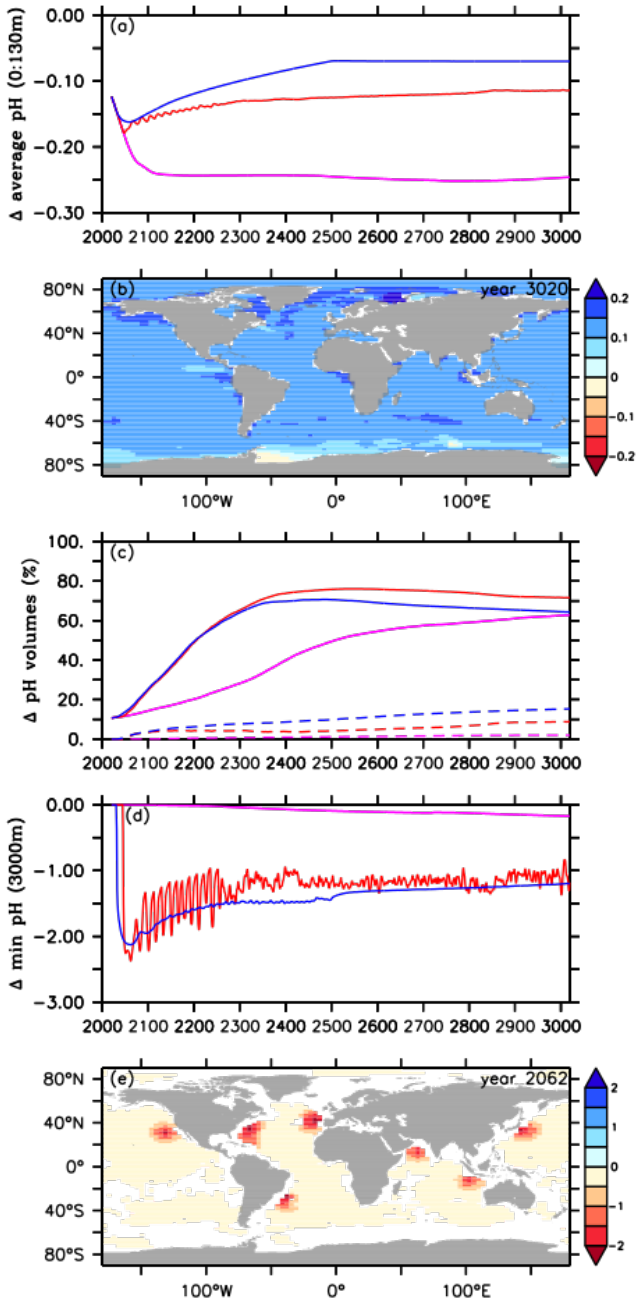

Figure 3: Comparison of pH values between the default RCP 4.5 control run (purple lines), the A2 simulation (red lines) and the A3 simulation (blue lines) for **(a)** average ocean surface pH (0 to 130 m depth), **(b)** difference in ocean surface pH, relative to preindustrial, between the A2 simulation and the default RCP 4.5 control run in yr 3020, **(c)** pH volumes of first (≤ 7.8 and ≥ 7.4, solid lines) and second category (< 7.4, dashed lines), **(d)** minimum pH values at 3000 m depth, and **(e)** difference in minimum pH at 3000 m depth between the A2 simulation and the default RCP 4.5 control run in yr 2062.

Earth Syst. Dynam. Discuss., https://doi.org/10.5194/esd-2018-87
Manuscript under review for journal Earth Syst. Dynam.
Discussion started: 1 March 2019

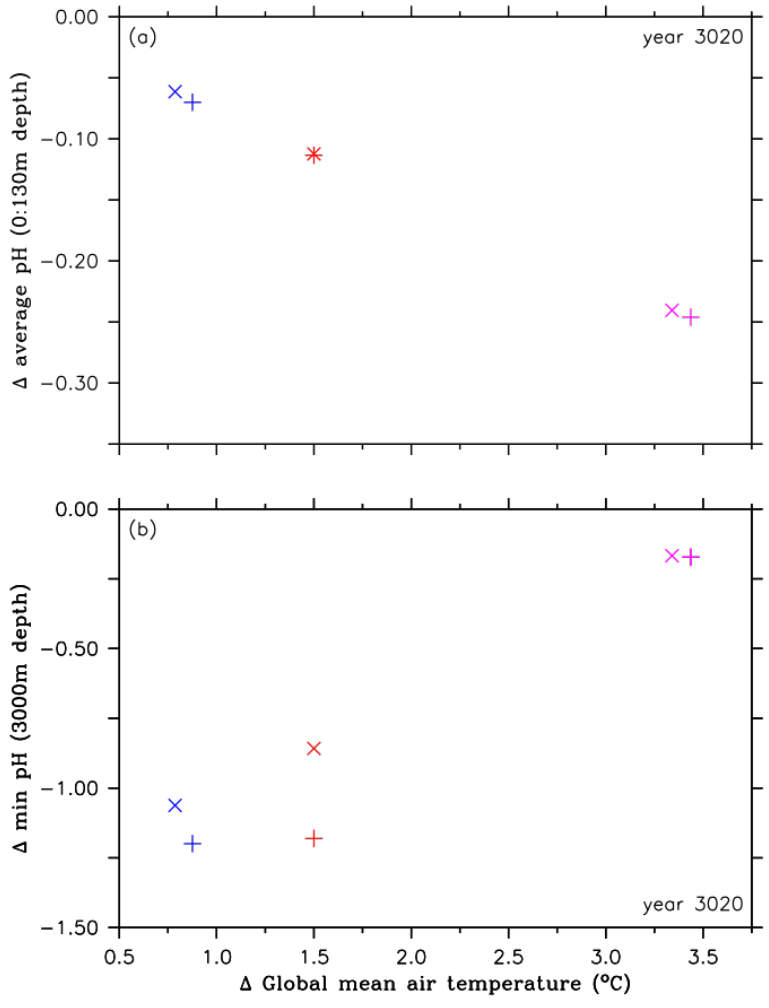

Figure 4: Comparison of pH values and corresponding global mean temperature in the year 3020, both relative to preindustrial, between the RCP 4.5 control simulations (purple symbols), simulations of the second approach (A2, red symbols) and simulations of the third approach (A3, blue symbols). The cross symbols refer to the default simulations and the X symbols denote simulations with $CaCO_3$ sediment and weathering feedbacks. These symbols represent for **(a)** changes in ocean surface pH (0 to 130m depth), relative to preindustrial, and **(b)** changes in minimum pH values at 3000 m depth, relative to preindustrial.

Earth Syst. Dynam. Discuss., https://doi.org/10.5194/esd-2018-87
Manuscript under review for journal Earth Syst. Dynam.
Discussion started: 1 March 2019

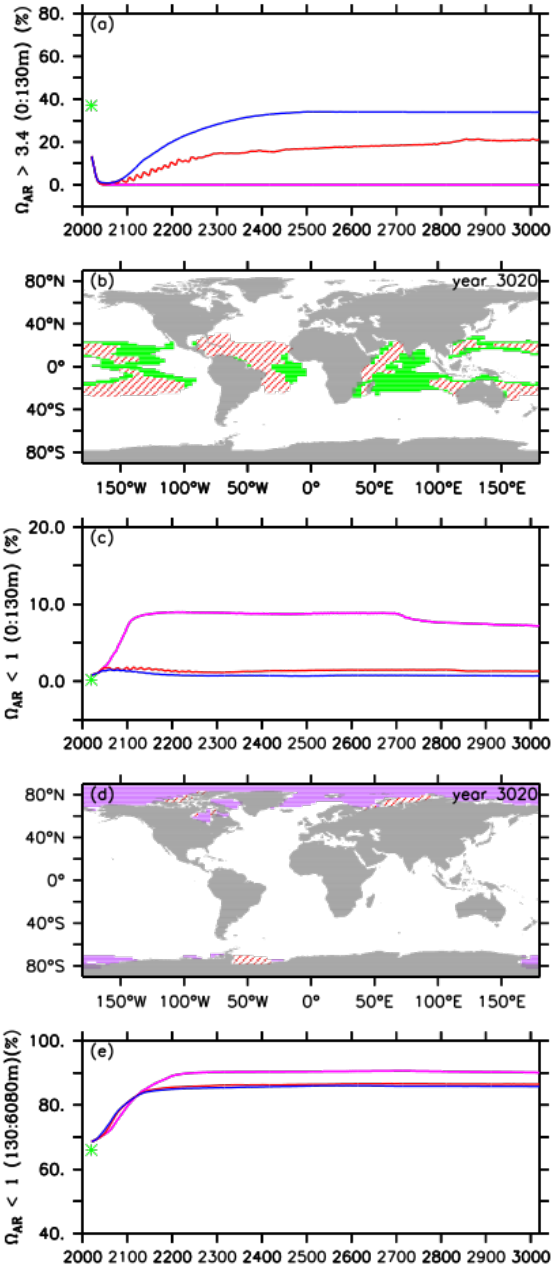

Figure 5: Comparison of volumes for different saturation states between preindustrial (green stars), the default RCP 4.5 control run (purple lines), the A2 simulation (red lines), and the A3 simulation (blue lines) for **(a)** omega aragonite > 3.4 in the upper ocean (0 to 130m depth), **(b)** potential coral reef habitat defined as the volume of the global upper ocean (0 to 130m depth) with omega aragonite > 3.4 and ocean temperatures between 21°C and 28°C for preindustrial (green) and the A2 simulation (red hatching) in in the year 3020, **(c)** omega aragonite < 1 in the upper ocean (0 to 130m depth), **(d)** global distribution of omega aragonite < 1 for the default control run (purple) and the A2 simulation (red hatching), and **(e)** omega aragonite < 1 in the intermediate and deep ocean (130 to 6080m depth).

770

Earth Syst. Dynam. Discuss., https://doi.org/10.5194/esd-2018-87
Manuscript under review for journal Earth Syst. Dynam.
Discussion started: 1 March 2019

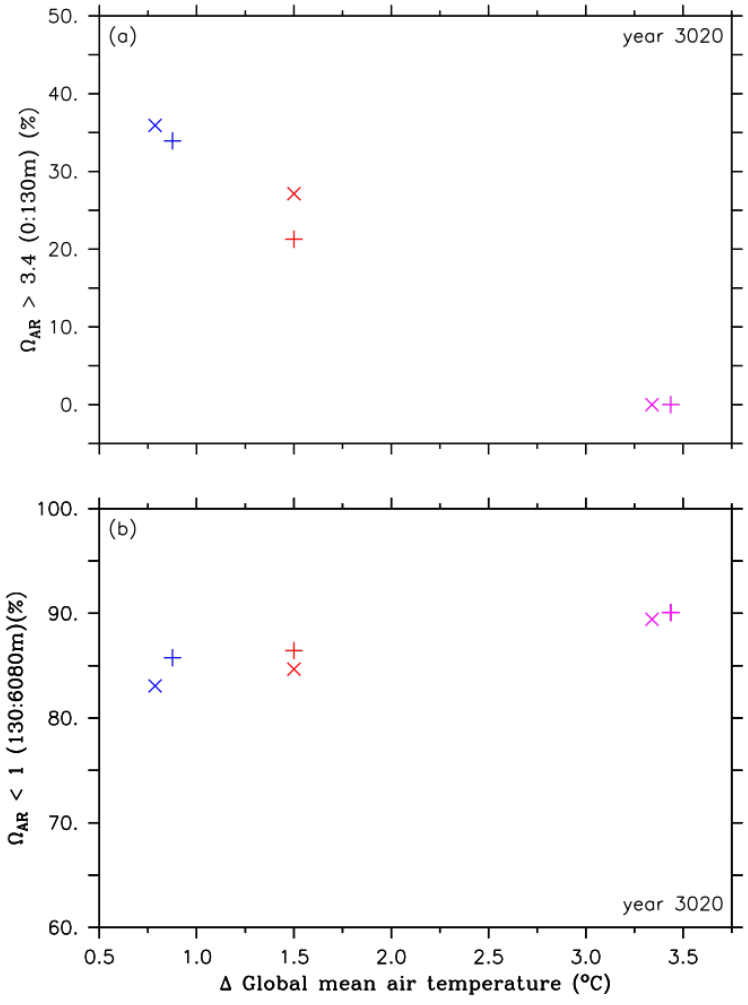

Figure 6: Comparison of volumes for different aragonite saturation states and corresponding global mean temperature in the year 3020, both relative to preindustrial, between the RCP 4.5 control simulations (purple symbols), simulations of the second approach (A2, red symbols) and simulations of the third approach (A3, blue symbols). The cross symbols refer to the default simulations and the X symbols denote simulations with $CaCO_3$ sediment and weathering feedbacks. These symbols represent for **(a)** omega aragonite > 3.4 in the upper ocean (0 to 130m depth), relative to preindustrial, and **(b)** changes in minimum pH values at 3000 m depth, relative to preindustrial.